Nanoscale

PAPER

View Article Online
View Journal | View Issue

Cite this: *Nanoscale*, 2023, **15**, 11491

Uniform nucleation and growth of $Cs_3Cu_2I_5$ nanocrystals with high luminous efficiency and structural stability and their application in white light-emitting diodes†

Zirui Liu,‡[a] Wei Li,‡[a] Lin Wang, *[a] Fei Zhang,[b] Sheng Wang,[a] Junchuan Liu,[a] Chengxi Zhang,[a] Luqiao Yin,[a] Guohua Jia, [c] Zhifeng Shi *[b] and Xuyong Yang *[a]

Received 31st May 2023,
Accepted 10th June 2023

DOI: 10.1039/d3nr02542j

rsc.li/nanoscale

Copper-based ternary halide composites have attracted great attention due to their superior chemical stability and optical properties. Herein, we developed an ultrafast high-power ultrasonic synthesis strategy to realize the uniform nucleation and growth of highly luminescent and stable $Cs_3Cu_2I_5$ nanocrystals (NCs). The as-synthesized $Cs_3Cu_2I_5$ NCs show uniform hexagonal morphology with an average mean size of 24.4 nm and emit blue light with a high photoluminescence quantum yield (PLQY) of ~85%. Moreover, the $Cs_3Cu_2I_5$ NCs exhibit a remarkable stability during continuous eight times heating/cooling cycling tests (303–423 K). We also demonstrated an efficient and stable white light-emitting diode (WLED) with a high luminous efficiency (LE) of 41.5 lm W^{-1} and a Commission Internationale de l'Eclairage (CIE) color coordinate of (0.33,0.33).

1 Introduction

Lead halide perovskite nanocrystals (NCs) have been widely used in the field of light-emitting diodes (LEDs) due to their outstanding optoelectronic properties such as tunable emission wavelengths, high photoluminescence quantum yields (PLQYs), and narrow emission line widths.[1–13] To date, the external quantum efficiencies (EQEs) of perovskite-based LEDs have exceeded over 20%, showing great potential in next-generation displays and lighting.[14–20] However, their intrinsic heavy-metal toxicity and instability seriously restrict their practical application.[21–24] Recently, copper(I)-based halide $Cs_3Cu_2I_5$ NCs have emerged as a promising substitute for lead halides due to their relatively low toxicity, Earth-abundant composition and unique optoelectronic properties, such as high emission stability, low self-absorption and self-trapped exciton (STE) emission.[25–28]

To date, the most adopted strategy for synthesizing $Cs_3Cu_2I_5$ NCs is the hot-injection method, which highly relies on high reaction temperatures and organic phase media to facilitate crystallization and reduce defect states. Moreover, the crystalline phase, morphology, size and uniformity of the final NC products will be influenced by the temperature. For instance, by simply increasing the injection temperature from 70 °C to 110 °C, Cheng *et al.* used the same reactants and ligands to prepare 0D $Cs_3Cu_2I_5$ NCs and 1D $CsCu_2I_3$ nanorods with PLQYs of 67% and 5%, respectively.[26] To ensure the phase purity of $Cs_3Cu_2I_5$ NCs, Lian *et al.* and Gao *et al.* introduced indium iodide (InI_3) as a precursor into the hot-injection reaction system to inhibit the growth of the $CsCu_2I_3$ phase at high temperature (180 °C) by providing a halogen-rich environment, which also favours the elimination of iodide vacancies, leading to enhanced PLQY of 73.7% and 96.6%, respectively.[29,30] Meanwhile, although some impressive progress has been made in the applications of $Cs_3Cu_2I_5$ NCs in LEDs, ultraviolet (UV) photodetectors, X-ray imaging and anticounterfeiting technology,[26,31–33] their further development and industrial production are hindered by the high cost and complicated hot-injection process, which cannot guarantee the uniformity and reproducibility of $Cs_3Cu_2I_5$ NCs.[34,35]

Herein, we developed an ultrafast and efficient strategy to prepare high quality pure $Cs_3Cu_2I_5$ NCs on a large scale by employing a high-power ultrasonic system to provide pulse energy to guide the crystallization process. Under ultrasonic

[a]*Key Laboratory of Advanced Display and System Applications of Ministry of Education, Shanghai University, 149 Yanchang Road, Shanghai 200072, China. E-mail: lin_wang@shu.edu.cn, yangxy@shu.edu.cn*
[b]*Key Laboratory of Materials Physics of Ministry of Education, School of Physics and Microelectronics, Zhengzhou University, Daxue Road 75, Zhengzhou 450052, China. E-mail: shizf@zzu.edu.cn*
[c]*School of Molecular and Life Sciences, Curtin University, Perth, WA 6102, Australia*
†Electronic supplementary information (ESI) available. See DOI: https://doi.org/10.1039/d3nr02542j
‡These authors contributed equally to this work.

oscillation, abundant and uniform bubbles will be generated in the reaction solutions, which will facilitate the complete dissolution of precursors and the energy transfer in the reaction system for the uniform nucleation and growth of $Cs_3Cu_2I_5$ NCs. The as-synthesized $Cs_3Cu_2I_5$ NCs show uniform hexagonal morphology with an average mean size of 24.4 nm and a high PLQY of ~85%. Notably, the $Cs_3Cu_2I_5$ NCs exhibit remarkable luminescence and structural stability during eight times continuous heating/cooling cycles (303–423 K) and storage under an ambient atmosphere for over two months. We utilized the as-synthesized $Cs_3Cu_2I_5$ NCs in a white LED (WLED), for which the luminous efficiency (LE) is 41.5 lm W^{-1}, the color coordinates are (0.33,0.33), the correlated color temperature (CCT) is 5489 K, and the color rendering index (CRI) is 95.3. In addition, the operational stability of the WLED was also studied, and it can work in the air for over 180 min, suggesting outstanding stability.

2 Results and discussion

The specific synthesis processes are schematically illustrated in Fig. 1. Typically, Cs-oleate and CuI precursors were dissolved in *n*-octane as the precursor solution, into which an ultrasonic probe (800 W) was inserted directly to induce the oscillation of the reaction system. During the oscillation treatment, the generated abundant and uniform bubbles will release energy to cause the homogeneous reaction of precursors, and the $Cs_3Cu_2I_5$ NCs are formed when the mixture turns blue. The growth process can be terminated immediately by turning off the ultrasonic probe. The pure $Cs_3Cu_2I_5$ NC products on the ten gram scale were obtained after purification and exhibit bright blue emission under UV lamp (254 nm) irradiation.

X-ray diffraction measurement was performed to investigate the crystal structure of the as-prepared $Cs_3Cu_2I_5$ NCs (Fig. S1†). The diffraction peaks at 24.02°, 25.58°, 26.32°, and 30.62° can be assigned to the (122), (320), (222), and (004) planes of the orthorhombic $Cs_3Cu_2I_5$ NCs (JCPDS #450077, space group of *Pnma*), respectively,[36,37] indicating the pure $Cs_3Cu_2I_5$ phase. As shown in Fig. 2a, the as-synthesized $Cs_3Cu_2I_5$ NCs display uniform and hexagonal morphology with

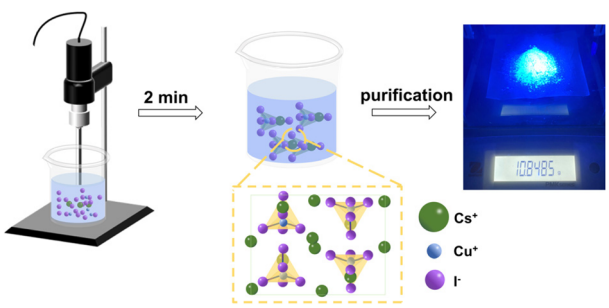

Fig. 1 Schematic diagram of the ultrafast ultrasound-assisted synthesis strategy for blue light-emitting $Cs_3Cu_2I_5$ NCs.

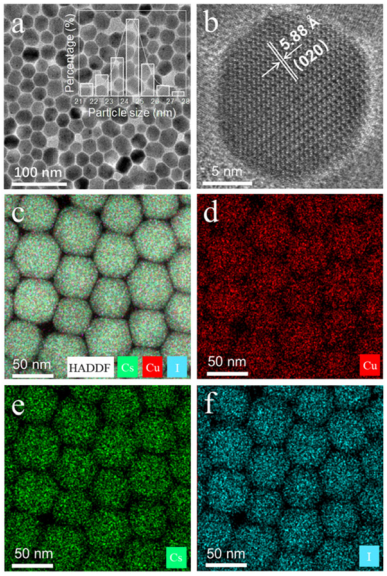

Fig. 2 (a) TEM and (b) HRTEM images of $Cs_3Cu_2I_5$ NCs. (c) HADDF-STEM measurement of NCs, and the corresponding EDS mapping of elemental (d) Cu, (e) Cs, and (f) I distributions.

an average mean size of 24.4 nm. According to the high-resolution TEM (HRTEM) image shown in Fig. 2b, a distinct lattice fringe can be observed with a lattice spacing of 5.88 Å, which corresponds to the interplanar distance of the (020) crystal phase of $Cs_3Cu_2I_5$. Fig. 2c–f are the elemental mapping images of $Cs_3Cu_2I_5$, where Cs, Cu, and I elements are uniformly distributed with a Cs : Cu : I atomic ratio of 29.66 : 24.28 : 46.06 (Table S1†). This is in accordance with the stoichiometric ratio of $Cs_3Cu_2I_5$. We further varied the reaction time from 1 min to 10 min to investigate the influence of the reaction time on the morphology of $Cs_3Cu_2I_5$ products. As shown in Fig. S2,† when reacting for 1 min, the growth process is still uncompleted and the morphology of the NCs is irregular; when reacting for 10 min, the morphology of the $Cs_3Cu_2I_5$ product remains nearly unchanged, which may be due to the fact that the precursors reacted completely at 2 min.

The optical properties of the as-synthesized $Cs_3Cu_2I_5$ NCs were systematically characterized. There are two absorption peaks at 261 nm and 285 nm (Fig. 3a), according to which the optical band gap was calculated to be 4.08 eV (Fig. S3†). When excited by 285 nm UV light, broadband blue light emission with a peak at 441 nm and a full width at half maximum (FWHM) of 83 nm was observed. The corresponding PLQY reaches 85%. A large Stokes shift of 156 nm implies that the self-absorption of photons can be effectively suppressed, which is of great interest for scintillators and luminescent solar concentrators.[38–40] Such a large Stokes shift and the broad-band feature imply that the emission may be caused by the radiative recombination of self-trapped excitons (STEs).[41–43] Since the PL spectrum can be deconvoluted into two peaks at 418 nm (peak a) and 455 nm (peak b) (Fig. S4†), this may imply two STEs with different depths. Moreover, we

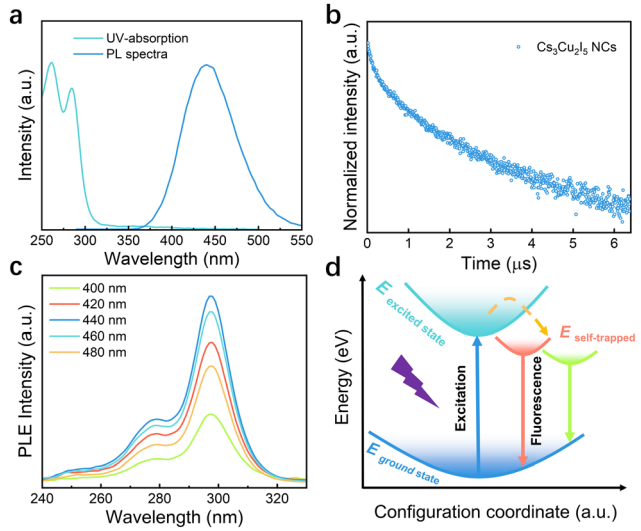

Fig. 3 Optical properties of $Cs_3Cu_2I_5$ NCs: (a) absorption and PL spectra, (b) TRPL spectra, and (c) PLE spectra at different emission wavelengths from 400 to 480 nm. (d) Schematic diagram of the emission from STEs.

compared the PL profiles and PLQYs of the $Cs_3Cu_2I_5$ NCs with those in previous reports. The PL peak positions are similar and the PLQYs are the highest for our $Cs_3Cu_2I_5$ NCs among all these NCs (Table S3†).

Time-resolved photoluminescence (TRPL) measurement was performed to gain more insight into the exciton recombination dynamics (Fig. 3b). The PL decay curve can be well fitted by a bi-exponential function, namely $I(T) = A_1 \exp(-t/\tau_1) + A_2 \exp(-t/\tau_2) + I_0$, where τ_1 and τ_2 are two kinds of lifetimes and A_1 and A_2 are used as coefficients to indicate the proportion. The τ_1 and τ_2 are 124 ns and 1072 ns, respectively, and the A_1 and A_2 are 16% and 84%, respectively. Depending on the ratio and types of lifetimes, peaks a and b can be matched with τ_1 and τ_2, respectively. The average PL lifetime for the $Cs_3Cu_2I_5$ NCs is 1.05 μs. To better understand the emission origin of the $Cs_3Cu_2I_5$ NCs, PLE spectra were recorded with monitoring wavelengths of 400, 420, 440, 460, and 480 nm, respectively. The PLE curves shown in Fig. 3c show the same shape and peak positions at different emission wavelengths, indicating that the broad emission originates from the relaxation of the same excited states rather than band–edge recombination, ion luminescence, or defect-related luminescence.[29,44] In addition, the PL intensities increase when varying the excitation wavelength from 270 to 310 nm (Fig. S5†). The corresponding photophysical process describing the formation of STEs is plotted in Fig. 3d. Under the irradiation of UV light, the lattice of $Cs_3Cu_2I_5$ NCs will be distorted under the strong electron–phonon coupling due to the Jahn–Teller effect, leading to the reorganization of excited states. The STE states will form below the excited state. The photoexcited electrons will relax rapidly to the lower energy STE states through a strong and ultrafast electron–phonon coupling process, giving out blue light emission.

The optical and structural stabilities of $Cs_3Cu_2I_5$ NCs against UV irradiation, environmental storage, and heat were tested in detail. As shown in Fig. 4a, the PL intensities of $Cs_3Cu_2I_5$ NCs remain almost unchanged for 10 hours under continuous irradiation with UV light (365 nm). The insets are the bright fluorescence photos of these $Cs_3Cu_2I_5$ NC solutions taken at the initial and end stages of the irradiation process, indicating the robustness of blue emission. XRD measurements were employed to investigate the long-term storage stability of $Cs_3Cu_2I_5$ NCs without any encapsulation in an ambient environment (Fig. 4b). It shows that the crystal structure remains the same as that of a fresh $Cs_3Cu_2I_5$ NC sample after storing for 50 days (about 24 °C, 50.0–70.0% RH). Thermal stability tests were carried out by increasing the temperature from 30 °C to 150 °C for 8 cycles and monitoring the evolution of PL intensities. With the increase of temperature, the PL intensity decreases gradually due to the thermo-induced fluorescence quenching effect (Fig. 4c). Impressively, the PL intensity of these $Cs_3Cu_2I_5$ NCs can recover to 99% or more of its initial value after eight continuous heating/cooling cycles (Fig. 4d). Taking advantage of the excellent emission performance and stability of our $Cs_3Cu_2I_5$ NCs, we designed phosphor-type WLEDs for optoelectronic application demonstration (Fig. 5a). The WLEDs were fabricated by simply spin-coating blue $Cs_3Cu_2I_5$ NCs powder and commercial red phosphors ((Sr, Ca)$AlSiN_3$:Eu) and green phosphors ($(Sr, Ba)_2SiO_4$:Eu) onto a UV chip (310 nm) layer-by-layer. Fig. 5b presents the electroluminescence (EL) spectrum of this LED, which contains three emission peaks at 445 nm, 523 nm and 625 nm, respectively. The WLED exhibits a high CRI of 95.3 with a Commission International de l'Eclairage (CIE) coordinate of (0.33,0.33), which is standard white light emission, and the corresponding correlated color temperature (CCT) is 5489 K

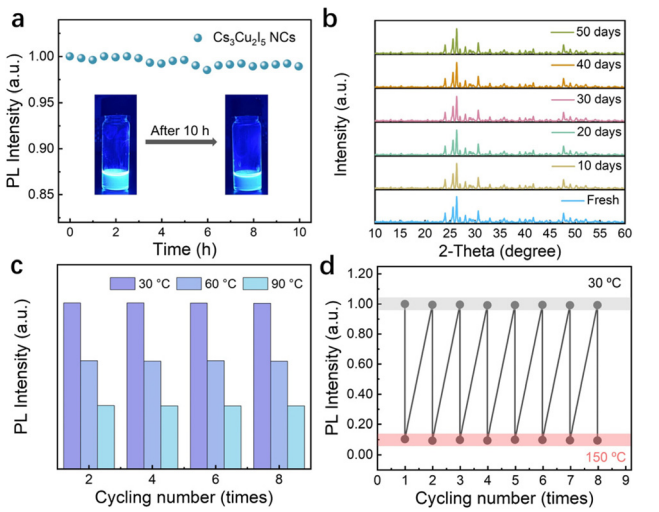

Fig. 4 Stability measurement of $Cs_3Cu_2I_5$ NCs: (a) PL stability of $Cs_3Cu_2I_5$ NCs, and the inset picture shows the sample under a 365 nm light source. (b) Structural stability of $Cs_3Cu_2I_5$ NCs with storage time. (c) PL intensities at selected temperatures and (d) the evolution of PL intensities during eight times thermal cycles.

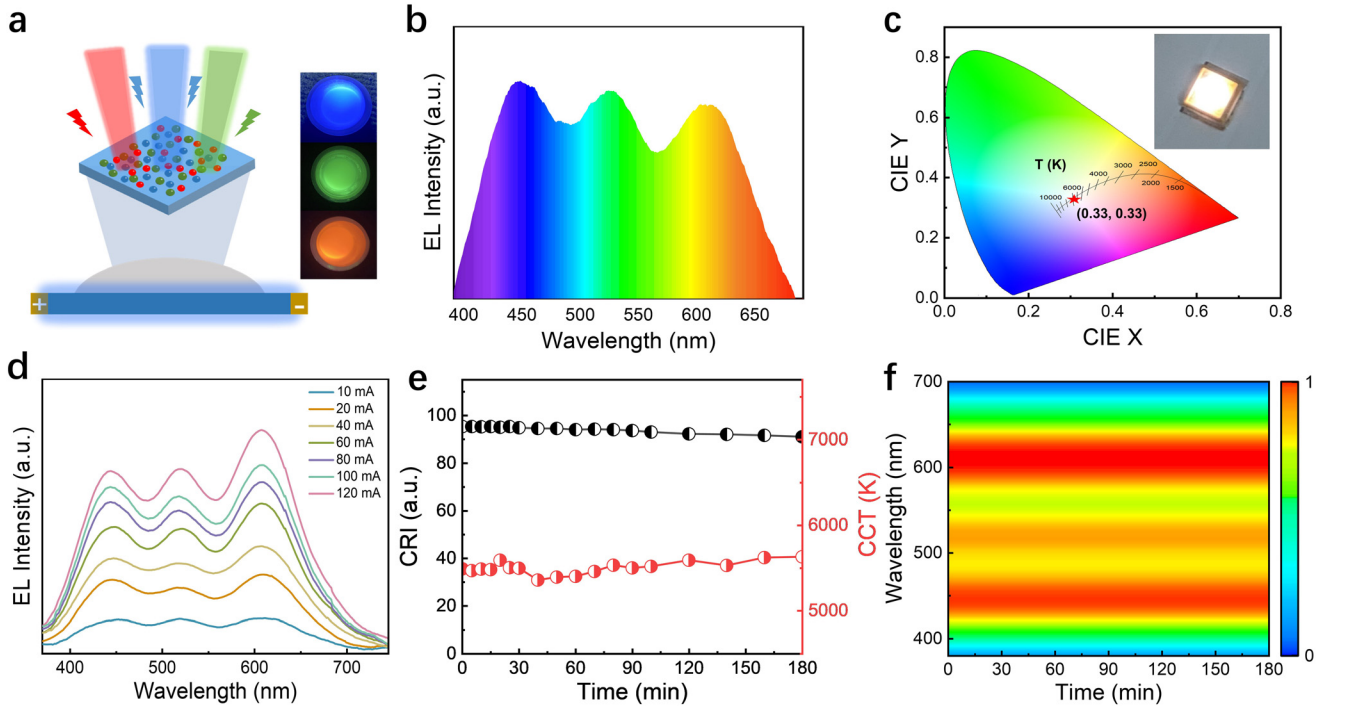

Fig. 5 (a) Schematic diagram of the device structure of the WLED. (b) EL spectrum of the WLED. (c) CIE coordinates for the WLEDs on the CIE1931 chromaticity chart and the photo of the WLED under operation (inset). (d) Emission spectra of the WLED under different driving currents. (e) The stability of CRI and CCT of the WLED under 10 mA operating current and (f) the corresponding EL spectra of the WLED.

(Fig. 5c). The luminous efficiency (LE) of the WLED prepared is 41.5 lm W^{-1}. The inset photograph shows a typical working device at a driving current of 30 mA and the light emission intensity increased gradually with the increase of the operating current (Fig. 5d). To evaluate the suitability of our WLED to practical applications, its operational stability was investigated in detail by tracking the evolution of the emission spectra. As shown in Fig. 5e, both CRI and CCT were continuously measured during the operation of the WLED for 180 min and showed no degradation. The corresponding emission spectra involving the spectral shape, peak position, and emission intensity remain unchanged (Fig. 5f), suggesting the superior operational stability of our WLED. We also summarized the performance parameters of WLEDs based on lead-free perovskites in Table S4,† among which the value of luminous efficiency of our WLED with a CRI of 95.3 is the highest.

3 Conclusions

We prepared high-quality blue light-emitting $Cs_3Cu_2I_5$ NCs by utilizing an ultrafast strategy assisted by an ultrasonic system. The ultrasonic probe provides uniform energy diffusion to guide the crystallization process. The obtained $Cs_3Cu_2I_5$ NCs have uniform morphology and size with a high PLQY of ~85%. Moreover, the structural and optical properties are demonstrated to be highly stable during heating/cooling tests and storage in an ambient environment. The WLEDs exhibit a CCT of 5489 K, a CRI of 95.3 and a LE of 41.5 lm W^{-1}. Impressively, the performance of the WLEDs shows negligible degradation after continuous operation for 180 min. Our work provides a new approach for the preparation of copper-based ternary halide nanocrystals.

4 Experimental

4.1 Materials and synthesis

Cesium carbonate (Cs_2CO_3, >98%) and oleylamine (OAm, 90%) were purchased from Acros. Copper(I) iodide (CuI, 99.999%) was acquired from Sigma. 1-Octadecene (ODE, technical grade, 90%) and oleic acid (OA, 90%) were purchased from Alfa Aesar. *n*-Octane (99.98%) was purchased from Sigma-Aldrich. Ethyl acetate (anhydrous 99.5%), *n*-hexane, isopropanol, and red ((Sr, Ca)$AlSiN_3$:Eu) and green ($(Sr, Ba)_2SiO_4$:Eu) phosphors were purchased from Beijing Chemical Reagent Ltd. Each precursor and solvent can be used without further purification.

4.2 Synthesis of $Cs_3Cu_2I_5$ NCs

Cs-oleate was prepared by dissolving Cs_2CO_3 (1.55 g) and OA (6.5 mL) in ODE (15 mL), which was degassed at 120 °C for 30 min under nitrogen. CuI (0.0762 g), ODE (5 mL), OA (0.5 mL) and OAm (0.5 mL) were degassed at 120 °C for 30 min under nitrogen until the CuI powder dissolved. Cs-oleate (0.8 mL, prepared as described above) and 10 mL *n*-octane were added to a beaker and the mixture was then sub-

jected to high power sonication under atmospheric conditions. The metal probe was placed into the solution at approximately 2 cm above the bottom of the beaker. The ultrasonication process lasted for 2 min and then stopped for 2 s after each 3 s of ultrasonication. As the sonication time increases, the color of the mixture changes, which indicates the formation of the $Cs_3Cu_2I_5$ halide solution. The original solution was centrifuged at 7500 rpm for 10 min to remove the supernatant, and finally, the $Cs_3Cu_2I_5$ powder for characterization was obtained. An ultrasound-assisted crusher (VCX800) with a nominal frequency of 20 kHz and a net output power of 800 W was used for the synthesis of $Cs_3Cu_2I_5$ halide solutions. NCs-HI was prepared by referring to previous work.[34]

4.3 Fabrication of WLEDs

The prepared blue emitting $Cs_3Cu_2I_5$ NCs, red phosphors, green phosphors and silica gel were mixed to obtain a homogeneous mixture. The WLED was fabricated onto a UV LED chip (310 nm) layer-by-layer. The device was cured in a vacuum oven at 40 °C for 60 min.

4.4 Characterization

The X-ray diffraction (XRD) patterns were recorded on a Rigaku Smartlab from 10° to 60°. The morphology of $Cs_3Cu_2I_5$ NCs was analysed by transmission electron microscopy (TEM, JEM-2100F, Cold Field Emission Type, JEOL). Energy-dispersive spectroscopy (EDS) was performed using TEM to analyse the elemental composition. The absorption spectra and transmittance were recorded using a PerkinElmer Lambda 950 UV-vis-NIR spectrometer. The absolute photoluminescence quantum yield (PLQY) and time-resolved fluorescence were measured by using an Edinburgh FLS920 spectrometer. The operational stability of WLEDs was tested using ZJZCL-1 OLED ageing lifespan test instrument. The performance of WLEDs was investigated using a Shenzhen Pynect integrated sphere (50 cm in diameter) system equipped with a Keithley 2400 source meter and a QEPro spectrograph.

Conflicts of interest

There are no conflicts to declare.

Acknowledgements

The authors would like to thank the financial support from the National Key Research and Development Program of China (2022YFE0200200), the National Natural Science Foundation of China (62174104, 61735004 and 52102182), the Program of Shanghai Academic/Technology Research Leader (22XD1421200), and the Shanghai Science and Technology Committee (22YF1413500).

References

1 Y. Jiang, C. Sun, J. Xu, S. Li, M. Cui, X. Fu, Y. Liu, Y. Liu, H. Wan, K. Wei, T. Zhou, W. Zhang, Y. Yang, J. Yang, C. Qin, S. Gao, J. Pan, Y. Liu, S. Hoogland, E. H. Sargent, J. Chen and M. Yuan, *Nature*, 2022, **612**, 679–684.
2 X. Du, L. Zhang, R. Chen, J. You, Y. Ma, J. Wang, Y. Wu, B. Liu, K. Zhao, J. Chen, X. Chen, Z. An and S. Liu, *Adv. Mater.*, 2022, **34**, 2207362.
3 J. Dong, F. Lu, D. Han, J. Wang, Z. Zang, L. Kong, Y. Zhang, X. Ma, J. Zhou, H. Ji, X. Yang and N. Wang, *Angew. Chem., Int. Ed.*, 2022, **61**, 202210322.
4 T. Wu, R. Zhao, J. Qiu, S. Wang, X. Zhang and Y. Hua, *Adv. Funct. Mater.*, 2022, **32**, 2204450.
5 Z. Ma, Z. Shi, D. Yang, Y. Li, F. Zhang, L. Wang, X. Chen, D. Wu, Y. Tian, Y. Zhang, L. Zhang, X. Li and C. Shan, *Adv. Mater.*, 2021, **33**, 2001367.
6 G. Na and L. Zhang, *Light: Sci. Appl.*, 2020, **9**, 106.
7 D. Pan, Y. Fu, N. Spitha, Y. Zhao, C. R. Roy, D. J. Morrow, D. D. Kohler, J. C. Wright and S. Jin, *Nat. Nanotechnol.*, 2021, **16**, 159–165.
8 Z. Chen, H. Xue, G. Brocks, P. A. Bobbert and S. Tao, *ACS Energy Lett.*, 2023, **8**, 943–949.
9 M. Fan, J. Huang, L. Turyanska, Z. Bian, L. Wang, C. Xu, N. Liu, H. Li, X. Zhang, C. Zhang and X. Yang, *Adv. Funct. Mater.*, 2023, **33**, 2215032.
10 C. Zhang, S. Wang, X. Li, M. Yuan, L. Turyanska and X. Yang, *Adv. Funct. Mater.*, 2020, **30**, 1910582.
11 H. Wang, X. Zhang, Q. Wu, F. Cao, D. Yang, Y. Shang, Z. Ning, W. Zhang, W. Zheng, Y. Yan, S. V. Kershaw, L. Zhang, A. L. Rogach and X. Yang, *Nat. Commun.*, 2019, **10**, 665.
12 H. Wang, X. Gong, D. Zhao, Y. Zhao, S. Wang, J. Zhang, L. Kong, B. Wei, R. Quintero-Bermudez, O. Voznyy, Y. Shang, Z. Ning, Y. Yan and E. H. Sargent, *Joule*, 2020, **4**, 1977–1987.
13 Y. Luo, L. Kong, L. Wang, X. Shi, H. Yuan, W. Li, S. Wang, Z. Zhang, W. Zhu and X. Yang, *Small*, 2022, **18**, 2200498.
14 J. Zhang, T. Zhang, Z. Ma, F. Yuan, X. Zhou, H. Wang, Z. Liu, J. Qing, H. Chen, X. Li, S. Su, J. Xie, Z. Shi, L. Hou and C. Shan, *Adv. Mater.*, 2023, **35**, 2209002.
15 Z. Liu, W. Qiu, X. Peng, G. Sun, X. Liu, D. Liu, Z. Li, F. He, C. Shen, Q. Gu, F. Ma, H. Yip, L. Hou, Z. Qi and S. Su, *Adv. Mater.*, 2021, **33**, 2103268.
16 Y. Dong, Y. Wang, F. Yuan, A. Johnston, Y. Liu, D. Ma, M. -J. Choi, B. Chen, M. Chekini, S. -W. Baek, L. K. Sagar, J. Fan, Y. Hou, M. Wu, S. Lee, B. Sun, S. Hoogland, R. Quintero-Bermudez, H. Ebe, P. Todorovic, F. Dinic, P. Li, H. T. Kung, M. I. Saidaminov, E. Kumacheva, E. Spiecker, L. -S. Liao, O. Voznyy, Z. -H. Lu and E. H. Sargent, *Nat. Nanotechnol.*, 2020, **15**, 668–674.
17 K. Lin, J. Xing, L. N. Quan, F. P. G. D. Arquer, X. Gong, J. Lu, L. Xie, W. Zhao, D. Zhang, C. Yan, W. Li, X. Liu, Y. Lu, J. Kirman, E. H. Sargent, Q. Xiong and Z. Wei, *Nature*, 2018, **562**, 245–248.

18 Y. Kim, S. Kim, A. Kakekhani, J. Park, Y. -H. Lee, H. Xu, S. Nagane, R. B. Wexler, D. -H. Kim, S. H. Jo, L. Martinez-Sarti, P. Tan, A. Sadhanala, G. -S. Park, Y. -W. Kim, B. Hu, H. J. Bolink, S. Yoo, R. H. Friend, A. M. Rappe and T. -W. Lee, *Nat. Photonics*, 2021, **15**, 148–155.
19 L. Kong, J. Wu, Y. Li, F. Cao, F. Wang, Q. Wu, P. Shen, C. Zhang, Y. Luo, L. Wang, L. Turyanska, X. Ding, J. Zhang, Y. Zhao and X. Yang, *Sci. Bull.*, 2022, **67**, 529–536.
20 L. Kong, Y. Luo, L. Turyanska, T. Zhang, Z. Zhang, G. Xing, Y. Yang, C. Zhang and X. Yang, *Adv. Funct. Mater.*, 2023, **33**, 2209186.
21 J. -M. Heo, H. Cho, S. -C. Lee, M. -H. Park, J. S. Kim, H. Kim, J. Park, Y. -H. Kim, H. J. Yun, E. Yoon, D. -H. Kim, S. Ahn, S. -J. Kwon, C. -Y. Park and T. -w. Lee, *ACS Energy Lett.*, 2022, **7**, 2807–2815.
22 J. Lu, X. Guan, Y. Li, K. Lin, W. Feng, Y. Zhao, C. Yan, M. Li, Y. E. Shen, X. Qin and Z. Wei, *Adv. Mater.*, 2021, **33**, 2104414.
23 L. Zhao, Q. Li, C. -H. Hou, S. Li, X. Yang, J. Wu, S. Zhang, Q. Hu, Y. Wang, Y. Zhang, Y. Jiang, S. Jia, J. -J. Shyue, T. P. Russell, Q. Gong, X. Hu and R. Zhu, *J. Am. Chem. Soc.*, 2022, **144**, 1700–1708.
24 F. Ye, Q. Shan, H. Zeng and W. C. H. Choy, *ACS Energy Lett.*, 2021, **6**, 3114–3131.
25 Z. Ma, Z. Shi, C. Qin, M. Cui, D. Yang, X. Wang, L. Wang, X. Ji, X. Chen, J. Sun, D. Wu, Y. Zhang, X. J. Li, L. Zhang and C. Shan, *ACS Nano*, 2020, **14**, 4475–4486.
26 P. Cheng, L. Sun, L. Feng, S. Yang, Y. Yang, D. Zheng, Y. Zhao, Y. Sang, R. Zhang, D. Wei, W. Deng and K. Han, *Angew. Chem., Int. Ed.*, 2019, **58**, 16087.
27 F. Zhang, Z. Zhao, B. Chen, H. Zheng, L. Huang, Y. Liu, Y. Wang and A. L. Rogach, *Adv. Opt. Mater.*, 2020, **8**, 1901723.
28 J. Xu, S. Guo, J. Qu, S. Xu, C. Wang, D. Ban and Y. Cui, *Nanoscale*, 2021, **13**, 9659–9667.
29 L. Lian, M. Zheng, W. Zhang, L. Yin, X. Du, P. Zhang, X. Zhang, J. Gao, D. Zhang, L. Gao, G. Niu, H. Song, R. Chen, X. Lan, J. Tang and J. Zhang, *Adv. Sci.*, 2020, **7**, 2000195.
30 F. Gao, X. Zhu, Q. Feng, W. Zhong, W. Liu, H. Xu and Y. Liu, *Nano Energy*, 2022, **98**, 107270.
31 J. Zhou, K. An, P. He, J. Yang, C. Zhou, Y. Luo, W. Kang, W. Hu, P. Feng, M. Zhou and X. Tang, *Adv. Opt. Mater.*, 2021, **9**, 2002144.
32 W. Liang, L. Wang, Y. Li, F. Zhang, X. Chen, D. Wu, Y. Tian, X. Li, C. Shan and Z. Shi, *Mater. Today Phys.*, 2021, **18**, 100398.
33 Y. Dou, S. Wang, C. Zhang, H. Luo, X. Li, H. Wang, F. Cao, P. Shen, J. Zhang and X. Yang, *Adv. Mater. Technol.*, 2020, **5**, 1901089.
34 H. Huang, J. Raith, S. V. Kershaw, S. Kalytchuk, O. Tomanec, L. Jing, A. S. Susha, R. Zboril and A. L. Rogach, *Nat. Commun.*, 2017, **8**, 996.
35 C. Ran, J. Xu, W. Gao, C. Huang and S. Dou, *Chem. Soc. Rev.*, 2018, **47**, 4581–4610.
36 F. Zeng, Y. Guo, W. Hu, Y. Tan, X. Zhang, J. Yang, Q. Lin, Y. Peng, X. Tang, Z. Liu, Z. Yao and J. Du, *J. Lumin.*, 2020, **223**, 117178.
37 F. Zhang, Z. Zhao, B. Chen, H. Zheng, L. Huang, Y. Liu, Y. Wang and A. L. Rogach, *Adv. Opt. Mater.*, 2020, **8**, 1901723.
38 N. Li, Z. Xu, Y. Xiao, Y. Liu, Z. Yang and S. Liu, *Adv. Opt. Mater.*, 2022, **10**, 2200983.
39 Q. Yao, J. Li, X. Li, X. Zheng, Z. Wang and X. Tao, *Adv. Opt. Mater.*, 2022, **10**, 2201161.
40 Y. Gu, X. Yao, H. Geng, G. Guan, M. Hu and M. Han, *ACS Appl. Mater. Interfaces*, 2021, **13**, 40798–40805.
41 C. Chen, Y. Lin, P. Lai, H. Lin, G. Tan, H. Lin and R. D. Schaller, *Adv. Opt. Mater.*, 2022, **10**, 2200005.
42 Y. Li, Z. Zhou, F. Sheong, Z. Xing, R. Lortz, K. Wong, H. H. Y. Sung, I. D. Williams and J. E. Halpert, *ACS Energy Lett.*, 2021, **6**, 4383–4389.
43 Z. Xing, Z. Zhou, G. Zhong, C. C. S. Chan, Y. Li, X. Zou, J. E. Halpert, H. Su and K. S. Wong, *Adv. Funct. Mater.*, 2022, **32**, 2207638.
44 X. Hu, Y. Li, Y. Wu, W. Chen, H. Zeng and X. Li, *Mater. Chem. Front.*, 2021, **5**, 6152–6159.